First-principles investigation of the bulk and low-index surfaces of $MoSe_2$

Hossein Mirhosseini[1,*] and Guido Roma[1,2]
[1]*Institute of Inorganic and Analytical Chemistry, Johannes Gutenberg University, 55122 Mainz, Germany*
[2]*CEA, DEN, Service de Recherches de Métallurgie Physique, F-91191, France*

Janos Kiss and Claudia Felser
Max-Planck-Institut für Chemische Physik fester Stoffe, 01187 Dresden, Germany
(Received 17 February 2014; revised manuscript received 17 April 2014; published 6 May 2014)

In the framework of density functional theory, the geometry, electronic structure, and magnetic properties of the bulk and low index surfaces of $MoSe_2$ have been studied. We have carried out calculations with various exchange-correlation functionals to select one which is able to describe the van der Waals (vdW) interactions and gives the best geometry compared with experiments. The inclusion of the vdW forces, however, does not guarantee a reliable description for the geometry of this compound: some vdW functionals strongly overestimate the interlayer distance, similar to GGA functionals. Our investigation shows that the recently introduced optB86b-vdW functional yields the best results for $MoSe_2$. The vdW functionals have less impact on the electronic structure: the differences between the band structures of the experimental atomic structure, calculated by the vdW-DF and PBE functionals are marginal. We have tried the HSE06 hybrid functional as well but the results are not satisfactory: the overestimated interlayer distance leads to a significant overestimation of the band gap. The band structure of the bulk and monolayer is calculated and by the analysis of the bands character the indirect to direct band-gap transition is explained. The surface energy, work function and band structure of the surfaces are calculated as well. The role of the $MoSe_2$ buffer layer in $Cu(In,Ga)Se_2$ based solar cells is discussed by considering the work function values.

DOI: 10.1103/PhysRevB.89.205301 PACS number(s): 71.15.Mb, 71.20.−b, 68.55.ag, 73.20.At

I. INTRODUCTION

Layered transition-metal dichalcogenides (TMDs) display distinct physical and chemical properties. It has been demonstrated that reducing the thickness of TMDs such as MoS_2, WS_2, and $MoSe_2$ results in an indirect to a direct band-gap transition [1–3]. The direct band gap is in the visible frequency range and is predicted to exhibit coupled spin-valley physics [4,5]. The edges of layered TMDs, due to the dangling bonds and vacancies [6], are active sites for many important catalytic reactions [7]. TMDs have been reported as catalyst for hydrogen evolution reaction [8] and hydrodesulfurization [9]. Another important application of these layered compounds is in $Cu(In,Ga)Se_2$ (CIGS) thin film solar cells. It is believed that the desired orientation of the $MoSe_2$ planes with respect to the Mo(110) substrate can improve the efficiency of CIGS solar cells [10–15].

The layered structure of 2H-$MoSe_2$ [16,17] (with AbABaB stacking sequence; A, B: Se atom layers; a, b: Mo atom layers) has the basic unit of $MoSe_6$ prism in which one Mo atom is located in the trigonal prismatic hole of six Se atoms, Fig. 1(a). The bonding within each charge-neutral layer is covalent while there is only a weak vdW interaction between the $MoSe_2$ layers. Due to weak vdW forces between the layers and general tendency to minimize the surface energy, cleaving of a $MoSe_2$ crystal results in the chemically inert (0001) surface. The $(10\bar{1}0)$ surface of $MoSe_2$ [Fig. 1(c)] is parallel to one of the faces of the $MoSe_6$ prism. The topmost layer of this surface exposes two parallel rows of unsaturated Mo and Se atoms. The study of Raybaud *et al.* [18] on the $(10\bar{1}0)$ surface of MoS_2 shows that S atoms exposed on the topmost layer are chemically inert, while the Mo atoms exposed in the adjacent row are prone to strongly interact with adsorbate. The $(11\bar{2}0)$ surface is perpendicular to one of the faces of the $MoSe_6$ prism, Fig. 1(d). The topmost layer of this surface exposes two parallel rows of $MoSe_2$ unit; two Se nearest neighbors of each Mo atom and one Mo nearest neighbor of each Se atom are missing.

Compared with the (0001) surface, relatively little is known about the structural and electronic properties of the $(10\bar{1}0)$ and $(11\bar{2}0)$ surfaces. This is mainly related to the natural difficulty in preparing these surfaces. Recently, however, Kong *et al.* [7] introduced a synthesis process to grow $MoSe_2$ thin films with vertically aligned layers. Depending on the experimental parameters, the formation of the (0001), $(10\bar{1}0)$, and $(11\bar{2}0)$ surfaces has been reported either by selenization of Mo films [19,20] or by growing $MoSe_2$ on different substrates [21]. Due to recently growing interest on $MoSe_2$ surfaces, a comprehensive study of $MoSe_2$ surfaces seems necessary. To the best of our knowledge, no calculation has been performed on the geometry and band structure of the $(10\bar{1}0)$ and $(11\bar{2}0)$ surfaces. In this study, our first aim is to find an exchange-correlation functional that can properly describe the geometry of $MoSe_2$. Then, using this functional, we study the properties of the bulk and surfaces.

The paper is organized as follows. Theoretical aspects are addressed in Sec. II, results are presented in Sec. III, and we summarize our results in Sec. IV.

II. THEORETICAL ASPECTS

The unit cell of the $MoSe_2$ bulk consists of six atoms, two Mo and four Se, and is repeated in x, y, and z directions.

*mirhosse@uni-mainz.de

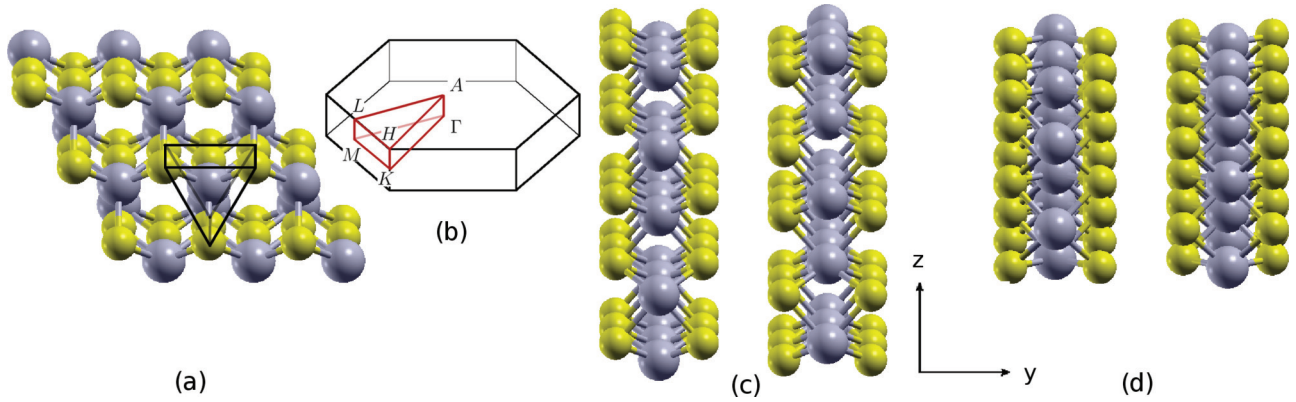

FIG. 1. (Color online) (a) Crystal structure of $MoSe_2$ bulk. The trigonal prism indicates the $MoSe_6$ basic unit with one Mo atom in the trigonal prismatic hole of six Se atoms. (b) First Brillouin zone of the hexagonal Bravais lattice along with the symmetry directions. (c) and (d) depict the $(10\bar{1}0)$ and $(11\bar{2}0)$ surfaces of $MoSe_2$. Surfaces are perpendicular to the z axis and the unit cell of each surface is repeated in x and y directions.

The $MoSe_2$ surfaces are modelled by periodically repeated slabs with two surfaces perpendicular to the z axis. The (0001) slab consists of 18 atoms and two others contain 48 atoms each. Slabs are separated from each other by 20 Å vacuum space. Parameters like kinetic energy cutoff, k-point grids, the thickness of vacuum space, and the number of layers have been tested to be sure that calculations are converged.

All calculations have been performed within the framework of density functional theory (DFT) implemented in the QUANTUM ESPRESSO (QE) package [22] and Vienna *ab initio* simulation package (VASP) [23]. The analysis of the structural stability has been carried out in two different ways: either by volume optimizations, i.e., the atomic positions are relaxed at a constant (zero) pressure, or by static lattice calculations, i.e., the ground-state energies of the structures with the given lattice parameters a and c are calculated and the collected data are fitted to an equation of state. In the first method, the relaxation relies also on the stress tensor, recently implemented for vdW functionals [24], while in the second method, the relaxation relies only on the calculation of total energy and forces.

For the calculations performed by VASP. we have used the projector augmented wave (PAW) [25,26] method together with a plane-wave cutoff energy of 400 eV (29.4 Ry) and $(9 \times 9 \times 3)$ k points. The Mo pseudopotential is chosen such that the $4p$ semicore states are treated as valence states. For the calculations performed by QE, the kinetic energy cutoff for wave functions and charge density were set to 55 and 300 Ry, respectively. For Brillouin zone integration, we use a $(9 \times 9 \times 3)$ k-point mesh for the bulk, a $(9 \times 9 \times 1)$ k-point mesh for the (0001) surface, a $(9 \times 3 \times 1)$ k-point mesh for the $(10\bar{1}0)$ surface, and a $(5 \times 3 \times 1)$ k-point mesh for the $(11\bar{2}0)$ surface. The structural relaxation is performed until the maximum force on each atom is less than 10^{-3} Ry/Bohr. The atomic pseudopotentials were generated by the atomic code included in the QE package and similar to our previous studies [27,28], the $4s$ and $4p$ semicore states of Mo are included in the pseudopotentials. We remark that in all vdW functionals containing nonlocal terms, the pseudopotentials are commonly generated using, instead of the nonlocal term, some gradient correction on correlation (for example with the revPBE exchange correlation functional for vdW-DF). Here, we chose to generate the pseudopotentials for optB86b-vdW and optB88-vdW without any gradient correction on correlation. However, further checks with pseudopotentials generated with a gradient correction on correlation [29] give even better results for the lattice parameters.

In order to benchmark the performance of various exchange-correlation functionals, we have carried out a set of calculations with VASP and QE. In both packages, different flavours of DFT, which can take into account the vdW forces, are implemented. We have carried out volume optimizations with different exchange-correlation functionals starting from the experimental atomic positions and cell parameters. The results of the calculations performed for the bulk are summarized in Table I. These data show that although the a parameter

TABLE I. Comparison between the $MoSe_2$ experimentally measured lattice parameters ($a = 3.299$ Å and $c = 12.938$ Å) [16] and the results obtained by applying different exchange-correlation functionals to optimize the cell volume. The Δa and Δc values show the differences between experimental and calculated values expressed in percentage. The calculated results are sorted based on the Δc values calculated by VASP: from the best agreement (top) to the worst agreement (bottom). The values in the brackets are calculated by static lattice calculations. It should be mentioned that the potential energy surface close to the equilibrium value of the parameter c is very flat. This leads to discrepancies between the equilibrium values of the parameter c calculated by different methods.

	VASP		QE	
	Δa (%)	Δc (%)	Δa (%)	Δc (%)
optB86b-vdW [34]	0.24	0.67	0.31 (0.33)	1.40 (1.61)
PBEsol [37]	−0.67	1.49	–0.55(–0.61)	2.30 (5.27)
optB88-vdW [34]	1.18	1.52	1.25	2.43
DFT-D2 [38]	0.64	1.98	0.83	1.09
optPBE-vdW [30]	1.42	3.88	...	...
vdW-DF2 [39]	4.57	7.54	4.79	5.29
HSE06 [40]	−0.24	7.57	...	...
PBE [41]	1.00	7.91	1.03	8.69
vdW-DF [31,32,42]	2.88	8.53	2.93 (2.91)	6.63 (8.62)

is rather well described by most functionals (except vdW-DF and vdW-DF2), the c parameter can be severely overestimated. The best agreement between experiment and theory is provided by the relatively new optB86b-vdW functional. The empirical DFT-D2 functional provides acceptable results as well.

From the data displayed in Table I, it is evident that the correct description of the vdW interaction between the $MoSe_2$ layers is crucial for the structure optimization. The commonly used exchange-correlation functionals are "short-sighted" [30] and cannot describe vdW interactions. In the vdW-density functional [31,32], the exchange-correlation energy takes the form of

$$E_{XC} = E_X + E_C^{LDA} + E_C^{nl}, \quad (1)$$

where E_X is the exchange energy, and E_C^{LDA} is the local density approximation (LDA) to the correlation energy. E_C^{nl} is the nonlocal part of the correlation energy, which is obtained by computing the double spatial integral of the ground-state electronic density. In the original vdW-DF [32], E_X is chosen to be the exchange part of the revPBE functional [33]. But vdW-DF overestimates the c parameter of $MoSe_2$ by about 8.5 %, Table I. As it has been pointed out [34], this is mainly due to the selected exchange functional. A remedy for this problem, based on the optimization of the exchange functionals, was proposed by Klimeš *et al.* [30]. Previous studies on layered structures show the good performance of these optimized functionals [35,36]. Among the different functionals that have been tested, we have used the optB86b-vdW functional, which has been implemented into QE by us, for most calculations of this work. When it was not applicable, we have used other functionals. In particular, for calculations including spin-orbit coupling, presently not implemented in QE for vdW-functionals, we have used the PBEsol exchange correlation functional together with fully relativistic pseudopotentials generated with the same parameters (atomic configuration, radii, reference energies) as in the other cases.

III. RESULTS AND DISCUSSION

A. $MoSe_2$ bulk

To calculate the bulk lattice parameters and the interlayer binding energy, first the optimum value of a for given values of c is calculated. Then to achieve the best value of c, the set of energy versus c data is fitted to the Morse potential energy function. In Fig. 2, the variation of the interlayer binding energy as a function of the lattice parameter c is shown. We have examined four different exchange-correlation functionals: PBE, PBEsol, vdW-DF, and optB86b-vdW. The reference energy for each curve is the total energy of the bulk with a large value of the interlayer distance ($c = 30$ Å) calculated with the selected functional.

As we have seen in the previous section, the optB86b-vdW functional predicts the best values of the lattice parameters. The unexpected result, however, is the difference between PBE and PBEsol curves. Namely, PBE predicts the monolayers of $MoSe_2$ to be more stable than the $MoSe_2$ bulk while the PBEsol curve has a minimum. PBE and PBEsol are at the same level of the DFT theory and one expects a similar behavior from these functionals. The prediction of the stability of the $MoSe_2$ bulk by PBEsol is a result of the optimization

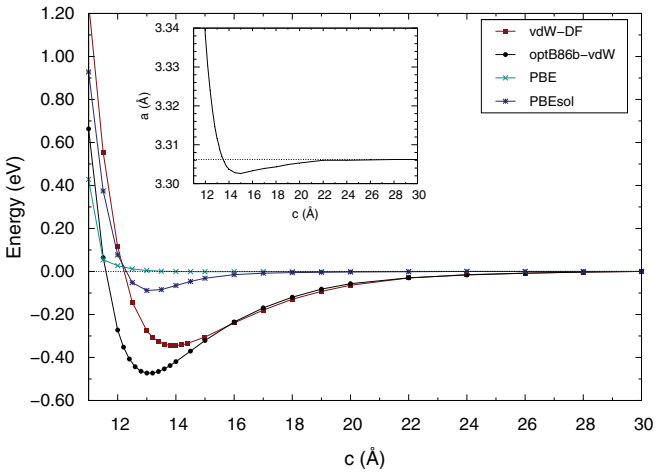

FIG. 2. (Color online) Variation of the interlayer interaction energy and the lattice parameter a (inset) as a function of the interlayer distance. The reference energy ($E = 0$) is defined as the total energy of the bulk with $c = 30$ Å calculated with the selected functional.

of the exchange part of this functional. The attraction between the layers comes from the exchange contribution and is only a coincidence [43]. The calculated interlayer interaction by PBEsol, however, is very small. Comparing the interlayer binding energies, optB86b-vdW gives the strongest binding energy: the binding energy calculated by optB86b-vdW (473 meV) is about five times larger than that calculated by PBEsol (83 meV) and about 1.4 times larger than that calculated by vdW-DF (345 meV). We note in passing that the DFT-D2 functional gives an interlayer binding energy (460 meV) close to optB86b-vdW. Using many-body perturbation theory and DFT techniques, Björkman *et al.* [44,45] have calculated the binding energies of large number of layered compounds including $MoSe_2$. Our binding energies (17.28 meV/Å^2 for vdW-DF and 22.22 meV/Å^2 for vdW-D2) are different but close to those calculated in Ref. [44] (15.33 meV/Å^2 for vdW-DF and 24.16 meV/Å^2 for vdW-D2). The main reason of this disagreement is probably the difference between the optimized structures. While our structures are fully relaxed for the chosen lattice parameters, the in-plane lattice parameters are fixed in Ref. [44]. The binding energy calculated using the optB86b-vdW functional (24.8 meV/Å^2) is 26% larger than the one calculated by the random phase approximation (19.63 meV/Å^2).

The inset of Fig. 2 shows the variation of the lattice parameter a with the lattice parameter c calculated by optB86b-vdW. A bulk with a larger c is expected to have a smaller value of a and vice versa [46]. But this is not true for the values of c between 15–22 Å. The lattice parameter a takes its minimum at $c = 15$ Å and grows with c until reaches its value for an isolated layer.

The indirect to direct band gap transition of MoS_2 and $MoSe_2$ has been shown experimentally and by calculations [1,3,46]. More interestingly, a sample of $MoSe_2$ with few layers has nearly degenerate indirect and direct band gap and a small change of the interlayer distance can drive the system towards the 2D limit [3]. To study the band gap transition, first we have optimized the structure of the bulk and monolayer and then

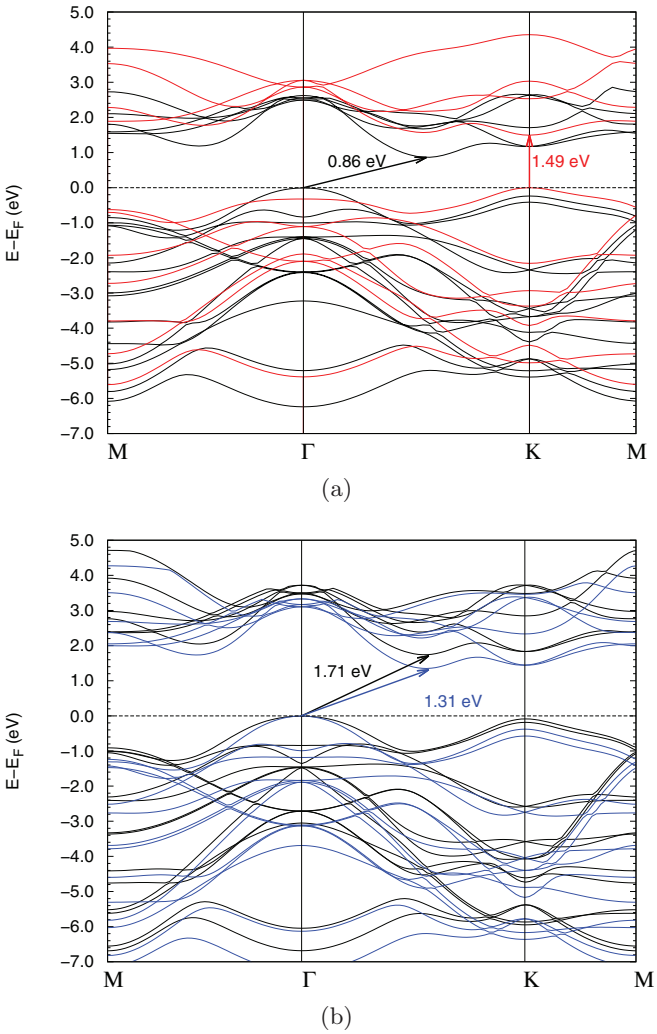

FIG. 3. (Color online) (a) Electronic structure of $MoSe_2$ bulk (black) and monolayer (red) calculated by optB86b-vdW. (b) Electronic structure of $MoSe_2$ bulk calculated by HSE06 functional for optimized structure (black) and experimental structure (blue). The bulk indirect band gap is shown by the black and blue arrows. The red arrow indicates direct band gap of the monolayer.

the band structures have been calculated, shown in Fig. 3(a). The bulk band structure shows a good agreement with the experimental and the previously calculated band structures [16,47,48]. The indirect band gap of the bulk has the value of 0.86 eV (0.24 eV smaller than the experimentally measured band gap [3]) and is shown by the black arrow in Fig. 3(a). The bulk band structure shows a 1.39 eV direct band gap at K (the experimental value is 1.42 eV [16]) and a 2.49 eV direct band gap at Γ. Reducing the number of layers from bulk to single layer is associated with changes in the band structure: the lowest point of the bulk conduction band between Γ and K moves upward, while the top of the bulk valence band at Γ shifts downward. In contrast, the size of the gap at K stays almost the same for the bulk and monolayer. Therefore, unlike the bulk, the monolayer of $MoSe_2$ is a semiconductor with a 1.49 eV direct band gap (0.06 eV smaller than the experimentally measured band gap [3]) at K [indicated by the red arrow in Fig. 3(a)].

We ought to mention, at this point, that the almost perfect agreement between the experimentally measured band gap of the *monolayer* and the band gap calculated by optB86b-vdW might be resulting from a compensation of errors. GW-BSE calculations [49,50] show that a large exciton binding energy is expected for the first absorption peak of the MoS_2 monolayer (the direct band gap). The inclusion of excitonic effects in the calculations reduces the size of the optical band gap, which is overestimated by GW, by almost 1 eV. A similar situation is expected for $MoSe_2$. Quasiparticle and excitonic effects are not included in the DFT calculations and the band gap of the monolayer, which is underestimated by DFT, coincides with the measured optical band gap. Conversely, in the case of the indirect band gap of the *bulk*, excitonic effects are expected to be negligible [49]. The bulk quasiparticle band gap is in good agreement with the experimental one but the underestimation of the band gap by DFT is moderate (∼20%).

The bands positions of layered systems like $MoSe_2$ are very sensitive to the distance between layers. The top of the valence band at Γ is a mixture of the Mo d_{z^2} and Se p_z orbitals while the same band at K is formed by hybridization of the Mo $d_{x^2-y^2}$ and d_{xy} orbitals with the Se p_x and p_y orbitals. The lower part of the conduction band is predominantly of Mo d character [47]. Varying the interlayer distance modifies the spatial overlap of the orbitals and consequently the dispersion and position of the bands. To examine the variation of the band gap with the interlayer distance, we have calculated the bulk band structure for two different geometries: bulk with experimental structure and bulk with the structure optimized by HSE06. The band structures are shown in Fig. 3(b). The interlayer distance of the optimized structure is about 7.5% larger than that of the experimental structure. The band gap for the optimized structure (1.71 eV) is about 30.0% larger than the band gap of the experimental structure (1.31 eV). Comparing the band structures shows that decreasing the interlayer distance causes a larger band dispersion around Γ, a downward shift of the conduction band and consequently a smaller band gap.

While some vdW functionals are able to describe the atomic structure of $MoSe_2$ accurately, the effect of these functionals on the band structure is insignificant. The band structures of the experimental structure calculated by PBE and vdW-DF, for example, are almost identical, i.e., vdW-functionals also underestimate the size of the bulk band gap. Hybrid functionals, designed to incorporate a portion of the exact exchange energy from Hartree-Fock method in the Kohn-Sham exchange-correlation energy, are popular for improving the band gaps, which are often underestimated by LDA and GGA. To explore the impact of the hybrid functionals on the electronic structure we have carried out a set of band-structure calculations for the experimental geometry with the HSE06 functional. For these calculations, we have used the standard value of the range-separation parameter (0.2 Å^{-}1) and different values of the exact-exchange (EE) fraction (default value for HSE06 is EE = 0.25). The results are summarized in Table II. By tuning EE values, it is possible to attain an indirect band gap very close to the experimental one (1.1 eV). But finding an optimum value of EE which can provide acceptable values for the direct and indirect band gaps is not feasible. This might be related to the fact that direct and indirect optical transitions contain different

TABLE II. Calculated band gaps (in eV) for the $MoSe_2$ bulk as a function of the exact-exchange fraction (EE) computed with the HSE hybrid functional for the experimental atomic structure and cell volume.

EE	indirect gap	direct gap at K	gap at Γ
0.25	1.31	1.81	3.09
0.20	1.22	1.74	2.92
0.15	1.09	1.65	2.79
0.10	1.00	1.55	2.64
0.05	0.90	1.47	2.51

contributions from excitonic binding energies [51]. Capturing excitonic effects is beyond the reach of DFT calculations (hybrid functional calculations included). Therefore tuning EE values cannot improve the size of direct and indirect band gap simultaneously. The foregoing discussions (considering the fact that HSE06 overestimates the lattice parameter c and band gap) suggest that the expensive HSE06 functional is not suitable to describe the geometry and band structure of $MoSe_2$, unless a suitable contribution coming from dispersion interaction is added [52].

B. $MoSe_2$ surfaces

Surfaces are modelled by slabs with two surfaces perpendicular to the z axis. The (0001) surface is created by breaking the vdW forces between layers, therefore all Se atoms exposed at the surface are saturated. Due to the lack of dangling bonds, this surface is a passive surface and shows a very small relaxation (0.027 Å). In contrast, the surfaces of $(10\bar{1}0)$ and $(11\bar{2}0)$ show corrugation. Atoms at the clean surface of $(10\bar{1}0)$ show large relaxation: the minimum energy of the clean $(10\bar{1}0)$ surface is obtained by 0.42-Å inward relaxation of the topmost Mo atoms and 0.028-Å outward relaxation of the topmost Se atoms. Compared with the $(10\bar{1}0)$ surface, the Mo and Se atoms at the $(11\bar{2}0)$ surface undergo smaller and larger relaxation, respectively. The minimum energy is obtained by 0.38-Å inward relaxation of the topmost Mo atoms and 0.11-Å outward relaxation of the topmost Se atoms.

Previous DFT calculations on the $(10\bar{1}0)$ surface of MoS_2 show that in each surface unit cell, migration of one S atom from the S-rich layer (S-terminated layer) to the S-poor layer (Mo-terminated layer) is energetically favourable [53]. Edges of (0001) surface resemble layers of $(10\bar{1}0)$ surface [54], where Mo-edge with 0% S coverage and S-edge with 100% S coverage correspond to the S-poor and S-rich layer of $(10\bar{1}0)$, respectively. The relaxed Mo-edge with 50% S coverage and S-edge with 50% S coverage have similar structure to the relaxed layers of the Mo50-S50 structure [53,54]. Regarding the $(10\bar{1}0)$ surface of $MoSe_2$, when one Se atom is removed from the Se-rich layer and is added to the Se-poor layer, a more stable structure is achieved. The relaxed structure of the new configuration gains 0.49 eV per $MoSe_2$ surface unit cell. Removing a Se atom from one layer of the $(11\bar{2}0)$ surface and adding it to the other one is accompanied by a major relaxation of the surface and the system gains 2.04 eV per surface unit cell. It is worth mentioning that removing S atoms from the S-rich layer of the $(10\bar{1}0)$ surface of MoS_2 is always a process with positive change in enthalpy [18] and could occur only for certain conditions in a reactor.

TABLE III. Calculated surface energies and work functions of different surfaces of $MoSe_2$. The values in the brackets are the surface energies and work functions of the surfaces after reconstruction.

Surface	Surface energy (J/m^2)	Work function (eV)
(0001)	0.21	5.19
$(10\bar{1}0)$	1.68 (1.49)	4.99 (5.20)
$(11\bar{2}0)$	1.83 (1.39)	4.93 (5.14)

The surface energy is calculated as the energy required to cleave a bulk crystal into two separate surfaces divided by the total area of the surfaces,

$$E_{\text{surface}} = \frac{E_{\text{slab}} - E_{\text{bulk}}}{A}, \tag{2}$$

where E_{slab} is the total energy of the slab, E_{bulk} is the total energy of the bulk with the same number of atoms in the slab, and A is the total surface area. The calculated surface energies listed in Table III show that the (0001) surface is the most stable and the $(11\bar{2}0)$ surface is the least stable one. The surface of $(10\bar{1}0)$ is more stable than $(11\bar{2}0)$ but its surface energy is much larger than the surface energy of (0001). The surface energy of the surfaces which are allowed to reconstruct (the values in the brackets) are smaller than the surface energy of the as-cleaved surfaces but these values are still far larger than the surface energy of the inert surface of (0001). The interesting result is that after reconstruction the $(11\bar{2}0)$ surface is more stable than $(10\bar{1}0)$. The surface energy comparison suggests that for free standing $MoSe_2$ slabs, only (0001) surface can form. But the presence of a substrate and growth conditions can dictate different orientation of $MoSe_2$ films. In general, if the growth rate is slow, the formation of $MoSe_2$ (0001) is more favorable than the other surfaces. But if the layers of $MoSe_2$ are formed rapidly, the $(10\bar{1}0)$ and $(11\bar{2}0)$ surfaces are formed [7,19,21].

Molybdenum is used as the back contact for CIGS solar cells. It is believed that formation of $MoSe_2$ layers between the Mo substrate and CIGS absorber yields ohmic contacts with good adhesion. To establish an Ohmic contact between the p-type CIGS absorber and the back contact, a metal with a work function larger than the work function of CIGS is needed [55]. Since Mo and most of the metals have work functions smaller than the CIGS work function, the formation of a Schottky barrier seems unavoidable. In this context, to understand the function of the $MoSe_2$ buffer layer, we need to compare the work function of the Mo(110) surface (4.78 eV) with the work functions of $MoSe_2$ surfaces, see Table III. The surface work functions are calculated as the difference between the vacuum level and the Fermi energy.[1] The former is estimated by the average of the electrostatic potential (excluding exchange correlation potential) in the vacuum space between slabs. The work function of Mo(110)

[1]The Fermi level of the (0001) surface is set to the top of the valence band.

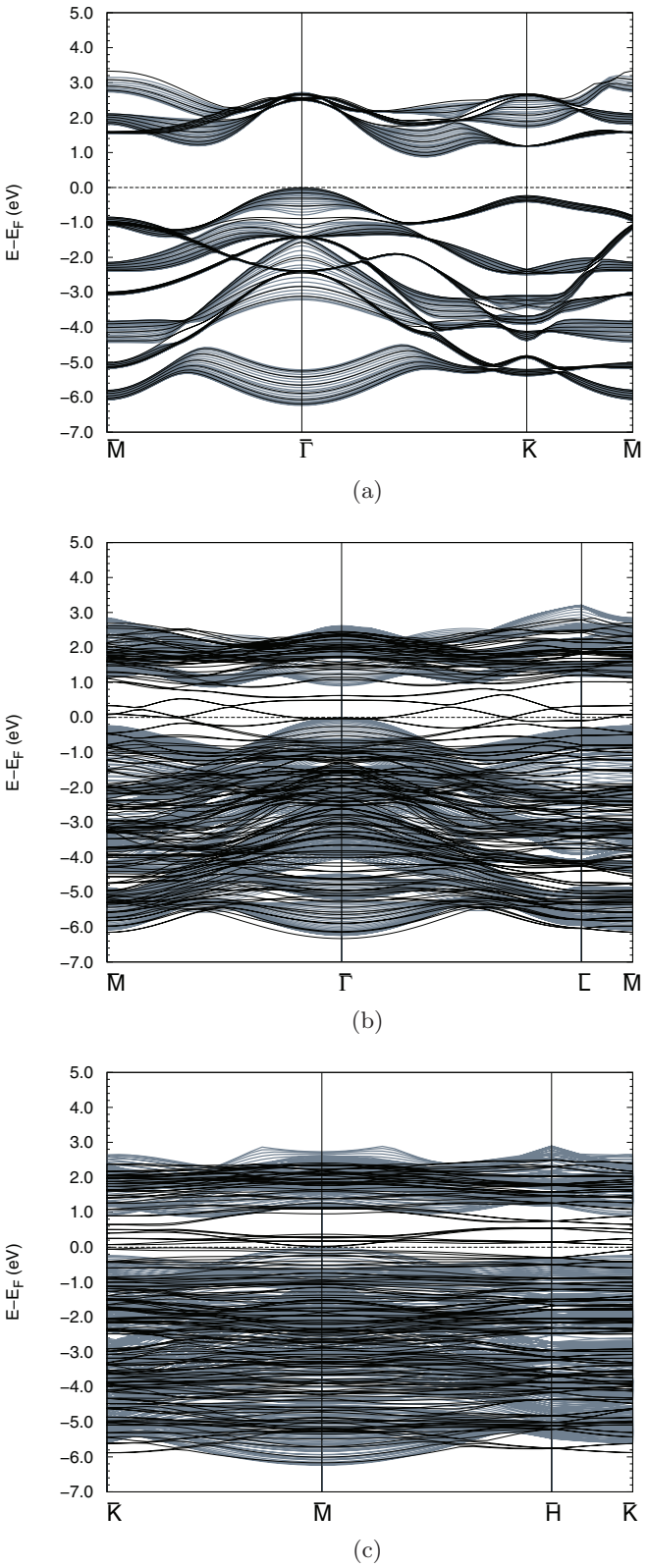

FIG. 4. (Color online) Band structure of the (a) (0001), (b) $(10\bar{1}0)$, and (c) $(11\bar{2}0)$ surfaces of $MoSe_2$ along high-symmetry directions, see Fig. 1(d). The grey-shaded area shows projected bulk bands.

is smaller than the work function of $MoSe_2$ surfaces, therefore the Mo/$MoSe_2$ interface is a Schottky barrier as well. But the interfacial barrier height varies by changing the orientation of the c-axis of $MoSe_2$ with respect to the Mo(110) surface. When the *c* axis is perpendicular to the Mo surface, the interfacial barrier height is larger than when the *c* axis is parallel to the Mo surface. This could affect the efficiency of the solar cells [56]. The work functions of the surfaces after reconstruction are also listed in Table III (the values in the brackets). Surface reconstructions result in larger values of the work function. It means if the reported reconstructions happen at the interface of Mo/$MoSe_2$, the efficiency of the solar cells will be reduced.

The surface band structures of the relaxed slabs are shown in Fig. 4. The (0001) band structure is similar to the bulk band structure; the band gap is indirect and practically identical with that of the bulk, although the slab contains only six MoSe2 layers (18 atoms). Compared with (0001) surface, the band structure of the other two surfaces show many surface states close to the Fermi level. In the case of the $(10\bar{1}0)$ surface, the projected bulk continuum presents a direct band gap, which might suggest the possibility of obtaining luminescence. However, since the coordination number of atoms at this

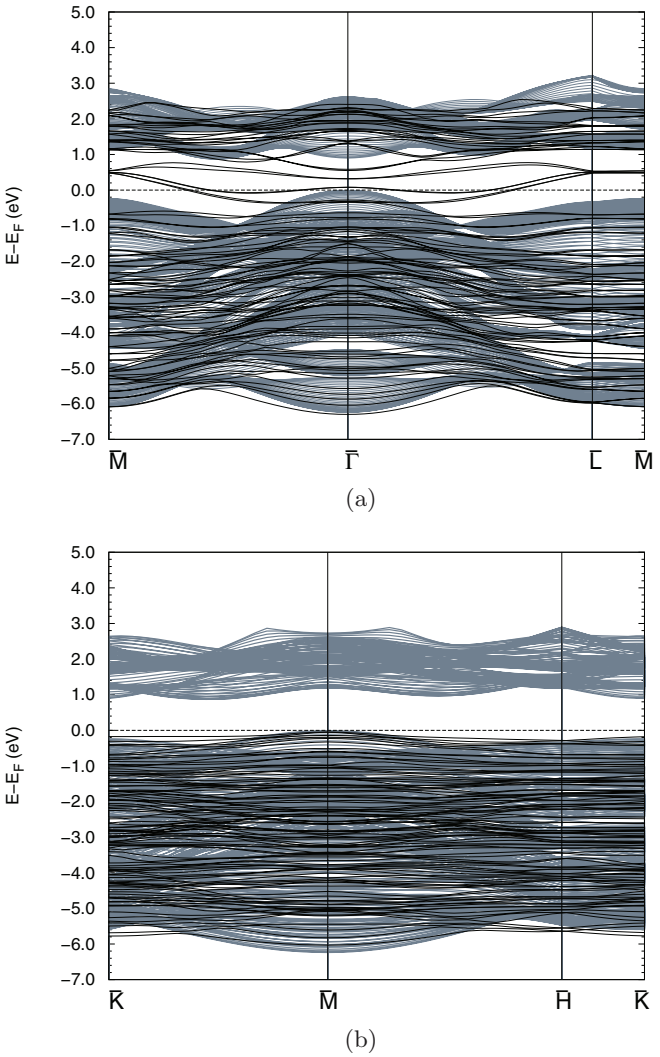

FIG. 5. (Color online) Band structure of the (a) $(10\bar{1}0)$, and (b) $(11\bar{2}0)$ surfaces of $MoSe_2$ along high-symmetry directions after reconstruction. The grey-shaded area shows projected bulk bands.

surface decreases, the band structure of the $(10\bar{1}0)$ surface shows a clearly metallic character. Surface reconstructions change the surface band structures, Fig. 5. By considering the reconstruction of the $(10\bar{1}0)$ surface, one expects to see only moderate changes in its band structure; the band structure shows a metallic character and there are surface states which cross the Fermi level. The changes in the band structure of $(11\bar{2}0)$ are, conversely, considerable. Similar to (0001), no surface state crosses the Fermi level and all unoccupied states are shifted far from the occupied ones.

It has been reported that Mo atoms at the zigzag edge of MoS_2 monolayer have finite magnetic moment [56–59]. The presence of the unsaturated edge atoms could be a reason for this unusual magnetic property. To study the magnetic properties of the bulk and surfaces, we have carried out spin-polarized calculations including spin-orbit coupling with the PBEsol functional, the second best for the geometry optimization according to Table I. To find out whether or not the bulk and surfaces of $MoSe_2$ have a magnetic ground state, we have compared the total energy of a system with finite initial magnetic moments and the total energy of a system in which all magnetic moments are forced to be zero. The bulk, (0001) and $(11\bar{2}0)$ surfaces have nonmagnetic ground state. In contrast, the $(10\bar{1}0)$ surface is a magnetic surface and the outermost unsaturated Mo atoms have finite magnetic moment. The total magnetic moment of the cell (consisting of 48 atoms) is $2.83\mu_B$. While there is no magnetic interaction between layers of the $(10\bar{1}0)$ surface, the Mo atoms within each layer are ferromagnetically ordered, with magnetic moments rapidly decreasing to zero in the bulk region. We note in passing that including spin-orbit coupling in band structure calculations, remove the degeneracy of bands. Here, for the sake of consistency, we have shown only the band structures calculated with the optB86b-vdW functional.

IV. SUMMARY AND OUTLOOK

In summary, we have tested different exchange-correlation functionals to find one suitable for the description of the $MoSe_2$ bulk structure. Among the recently proposed functionals, which are able to take into account vdW forces, optB86b-vdW predicts the atomic structure of $MoSe_2$ bulk very close to the experimental one. We have used this functional to calculate the geometry and band structure of the bulk and three surfaces. The electronic structure, nevertheless, is not improved by employing the vdW functionals: the bulk band structures calculated by PBE and vdW-DF show minor differences. The HSE06 hybrid functional, which is known to improve the values of the band gap, does not provide satisfactory atomic and electronic structure for $MoSe_2$.

By reducing the number of layers, the indirect to direct band-gap transition occurs. This is mainly because of the nature of the bands at the edges of the bulk band gap, which are very sensitive to the interlayer distance. The surface band structures are also calculated. The band structure of the (0001) surface is very similar to the bulk band structure, while the other two surfaces have a band structure more like a metal. This is the consequence of reducing the coordination number of surface atoms.

The different character of the $MoSe_2$ surfaces has certainly notable consequences on the properties of the devices containing $MoSe_2$ surfaces/interfaces, CIGS solar cells for example. It is out of the scope of the present paper to explain specific features of such devices. However, our results represent the first step towards a deeper understanding of the physics of devices based on $MoSe_2$ surfaces/interfaces.

ACKNOWLEDGMENTS

We acknowledge the financial support from the Federal Ministry for the Environment, Nature Conservation and Nuclear Safety for the comCIGS II project and Zentrum für Datenverarbeitung of Johannes Gutenberg University of Mainz for computing time.

[1] A. Splendiani, L. Sun, Y. Zhang, T. Li, J. Kim, C.-Y. Chim, G. Galli, and F. Wang, Nano Lett. **10**, 1271 (2010).
[2] H. R. Gutiérrez, N. Perea-López, A. L. Elías, A. Berkdemir, B. Wang, R. Lv, F. López-Urías, V. H. Crespi, H. Terrones, and M. Terrones, Nano Lett. **13**, 3447 (2013).
[3] S. Tongay, J. Zhou, C. Ataca, K. Lo, T. S. Matthews, J. Li, J. C. Grossman, and J. Wu, Nano Lett. **12**, 5576 (2012).
[4] D. Xiao, G.-B. Liu, W. Feng, X. Xu, and Wang Yao, Phys. Rev. Lett. **108**, 196802 (2012).
[5] K. F. Mak, K. He, J. Shan, and T. F. Heinz, Nat. Nanotechnol. **7**, 494 (2012).
[6] M. Bowker, Chem. Soc. Rev. **36**, 1656 (2007).
[7] D. Kong, H. Wang, J. J. Cha, M. Pasta, K. J. Koski, J. Yao, and Y. Cui, Nano Lett. **13**, 1341 (2013).
[8] D. Kong, J. J. Cha, H. Wang, H. R. Lee, and Y. Cui, Energy Environ. Sci. **6**, 3553 (2013).
[9] H. Topsøe, B. S. Clausen, and F. E. Massoth, in *Catalysis*, edited by J. Anderson and M. Boudart, Catalysis-Science and Technology Vol. 11 (Springer, Berlin, Heidelberg, 1996), pp. 1–269.
[10] S. Nishiwaki, N. Kohara, T. Negami, and T. Wada, Jpn. J. Appl. Phys. **37**, L71 (1998).
[11] T. Wada, N. Kohara, S. Nishiwaki, and T. Negami, Thin Solid Films **387**, 118 (2001).
[12] N. Kohara, S. Nishiwaki, Y. Hashimoto, T. Negami, and T. Wada, Sol. Energy Mater. Sol. Cells **67**, 209 (2001).
[13] R. Würz, D. F. Marrón, A. Meeder, A. Rumberg, S. Babu, T. Schedel-Niedrig, U. Bloeck, P. Schubert-Bischoff, and M. Lux-Steiner, Thin Solid Films **431**, 398 (2003).
[14] D. Abou-Ras, G. Kostorz, D. Bremaud, M. Kälin, F. Kurdesau, A. Tiwari, and M. Döbeli, Thin Solid Films **480**, 433 (2005).
[15] J. Pang, Y. Cai, Q. He, H. Wang, W. Jiang, J. He, T. Yu, W. Liu, Y. Zhang, and Y. Sun, Physics Procedia **32**, 372 (2012).
[16] T. Böker, R. Severin, A. Müller, C. Janowitz, R. Manzke, D. Voß, P. Krüger, A. Mazur, and J. Pollmann, Phys. Rev. B **64**, 235305 (2001).

[17] X. Huang, Z. Zeng, and H. Zhang, Chem. Soc. Rev. **42**, 1934 (2013).
[18] P. Raybaud, J. Hafner, G. Kresse, and H. Toulhoat, Surf. Sci. **407**, 237 (1998).
[19] A. Jäger-Waldau, M. Lux-Steiner, R. Jäger-Waldau, R. Burkhardt, and E. Bucher, Thin Solid Films **189**, 339 (1990).
[20] T. C. Bernede, J. Pouzet, and Z. K. Alaoui, Appl. Phys. A **51**, 155 (1990).
[21] A. Malloukyand and J. C. Bernede, Thin Solid Films **158**, 285 (1988).
[22] P. Giannozzi, S. Baroni, N. Bonini, M. Calandra, R. Car, C. Cavazzoni, D. Ceresoli, G. L. Chiarotti, M. Cococcioni, I. Dabo, A. D. Corso, S. de Gironcoli, S. Fabris, G. Fratesi, R. Gebauer, U. Gerstmann, C. Gougoussis, A. Kokalj, M. Lazzeri, L. Martin-Samos, N. Marzari, F. Mauri, R. Mazzarello, S. Paolini, A. Pasquarello, L. Paulatto, C. Sbraccia, S. Scandolo, G. Sclauzero, A. P. Seitsonen, A. Smogunov, P. Umari, and R. M. Wentzcovitch, J. Phys.: Condens. Matter **21**, 395502 (2009).
[23] G. Kresse and J. Furthmüller, Phys. Rev. B **54**, 11169 (1996).
[24] R. Sabatini, E. Küçükbenli, B. Kolb, T. Thonhauser, and S. de Gironcoli, J. Phys.: Condens. Matter **24**, 424209 (2012).
[25] P. E. Blöchl, Phys. Rev. B **50**, 17953 (1994).
[26] G. Kresse and D. Joubert, Phys. Rev. B **59**, 1758 (1999).
[27] G. Roma and L. Chiodo, Phys. Rev. B **87**, 245420 (2013).
[28] G. Roma, E. Ghorbani, H. Mirhosseini, J. Kiss, T. D. Kühne, and C. Felser, Appl. Phys. Lett. **104**, 061605 (2014).
[29] J. P. Perdew, Phys. Rev. B **33**, 8822 (1986).
[30] J. Klimeš, D. R. Bowler, and A. Michaelides, J. Phys.: Condens. Matter **22**, 022201 (2010).
[31] M. Dion, H. Rydberg, E. Schröder, D. C. Langreth, and B. I. Lundqvist, Phys. Rev. Lett. **92**, 246401 (2004).
[32] T. Thonhauser, V. R. Cooper, S. Li, A. Puzder, P. Hyldgaard, and D. C. Langreth, Phys. Rev. B **76**, 125112 (2007).
[33] Y. Zhang and W. Yang, Phys. Rev. Lett. **80**, 890 (1998).
[34] J. Klimeš, D. R. Bowler, and A. Michaelides, Phys. Rev. B **83**, 195131 (2011).
[35] H. Ding and B. Xu, J. Chem. Phys. **137**, 224509 (2012).
[36] G. Graziano, J. Klimeš, F. Fernandez-Alonso, and A. Michaelides, J. Phys.: Condens. Matter **24**, 424216 (2012).
[37] J. P. Perdew, A. Ruzsinszky, G. I. Csonka, O. A. Vydrov, G. E. Scuseria, L. A. Constantin, X. Zhou, and K. Burke, Phys. Rev. Lett. **100**, 136406 (2008).
[38] S. Grimme, J. Comput. Chem. **27**, 1787 (2006).
[39] K. Lee, E. D. Murray, L. Kong, B. I. Lundqvist, and D. C. Langreth, Phys. Rev. B **82**, 081101 (2010).
[40] J. Heyd, G. E. Scuseria, and M. Ernzerhof, J. Chem. Phys. **118**, 8207 (2003).
[41] J. P. Perdew, K. Burke, and M. Ernzerhof, Phys. Rev. Lett. **77**, 3865 (1996).
[42] G. Román-Pérez and J. M. Soler, Phys. Rev. Lett. **103**, 096102 (2009).
[43] D. C. Langreth, M. Dion, H. Rydberg, E. Schröder, P. Hyldgaard, and B. I. Lundqvist, Int. J. Quantum Chem. **101**, 599 (2005).
[44] T. Björkman, A. Gulans, A. V. Krasheninnikov, and R. M. Nieminen, Phys. Rev. Lett. **108**, 235502 (2012).
[45] T. Björkman, A. Gulans, A. V. Krasheninnikov, and R. M. Nieminen, J. Phys.: Condens. Matter **24**, 424218 (2012).
[46] C. Espejo, T. Rangel, A. H. Romero, X. Gonze, and G. M. Rignanese, Phys. Rev. B **87**, 245114 (2013).
[47] R. Coehoorn, C. Haas, J. Dijkstra, C. J. F. Flipse, R. A. de Groot, and A. Wold, Phys. Rev. B **35**, 6195 (1987).
[48] S. K. Mahatha, K. D. Patel, and K. S. R. Menon, J. Phys.: Condens. Matter **24**, 475504 (2012).
[49] T. Cheiwchanchamnangij and W. R. L. Lambrecht, Phys. Rev. B **85**, 205302 (2012).
[50] D. Y. Qiu, F. H. da Jornada, and S. G. Louie, Phys. Rev. Lett. **111**, 216805 (2013).
[51] H. Jiang, Phys. Chem. C **116**, 7664 (2012).
[52] G.-X. Zhang, A. Tkatchenko, J. Paier, H. Appel, and M. Scheffler, Phys. Rev. Lett. **107**, 245501 (2011).
[53] P. Raybaud, J. Hafner, G. Kresse, S. Kasztelan, and H. Toulhoat, J. Catal. **189**, 129 (2000).
[54] H. Schweiger, P. Raybaud, G. Kresse, and H. Toulhoat, J. Catal. **207**, 76 (2002).
[55] J. Spies, R. Schafer, J. Wager, P. Hersh, H. Platt, D. Keszler, G. Schneider, R. Kykyneshi, J. Tate, X. Liu, A. Compaan, and W. Shafarman, Sol. Energy Mater. Sol. Cells **93**, 1296 (2009).
[56] J.-H. Yoon, J.-H. Kim, W. M. Kim, J.-K. Park, Y.-J. Baik, T.-Y. Seong, and J.-h. Jeong, Prog. Photovoltaics **22**, 90 (2014).
[57] Y. Li, Z. Zhou, S. Zhang, and Z. Chen, J. Am. Chem. Soc. **130**, 16739 (2008).
[58] A. R. Botello-Méndez, F. López-Urías, M. Terrones, and H. Terrones, Nanotechnol. **20**, 325703 (2009).
[59] S. Tongay, S. S. Varnoosfaderani, B. R. Appleton, J. Wu, and A. F. Hebard, Appl. Phys. Lett. **101**, 123105 (2012).